iScience

CellPress

Article

ZnO Nanoparticles Encapsulated in Nitrogen-Doped Carbon Material and Silicalite-1 Composites for Efficient Propane Dehydrogenation

Dan Zhao, Yuming Li, Shanlei Han, ..., Jian Zhang, Binghui Ge, Evgenii V. Kondratenko

jianggy@cup.edu.cn (G.J.)
bhge@ahu.edu.cn (B.G.)
evgenii.kondratenko@catalysis.de (E.V.K.)

HIGHLIGHTS

Supported catalysts with stable ultrasmall ZnO nanoparticles were prepared

The N-doped carbon layer helps to protect ZnO NPs from sintering and volatilization

The catalysts exhibited excellent activity and stability in propane dehydrogenation

Zhao et al., iScience *13*, 269–276
March 29, 2019 © 2019 The Author(s).
https://doi.org/10.1016/j.isci.2019.02.018

iScience

CellPress

Article

ZnO Nanoparticles Encapsulated in Nitrogen-Doped Carbon Material and Silicalite-1 Composites for Efficient Propane Dehydrogenation

Dan Zhao,[1,5] Yuming Li,[1,5] Shanlei Han,[1] Yaoyuan Zhang,[1] Guiyuan Jiang,[1,6,*] Yajun Wang,[1] Ke Guo,[1] Zhen Zhao,[1] Chunming Xu,[1] Ranjia Li,[1] Changchun Yu,[1] Jian Zhang,[2] Binghui Ge,[3,*] and Evgenii V. Kondratenko[4,*]

SUMMARY

Non-oxidative propane dehydrogenation (PDH) is an attractive reaction from both an industrial and a scientific viewpoint because it allows direct large-scale production of propene and fundamental analysis of C-H activation respectively. The main challenges are related to achieving high activity, selectivity, and on-stream stability of environment-friendly and cost-efficient catalysts without non-noble metals. Here, we describe an approach for the preparation of supported ultrasmall ZnO nanoparticles (2–4 nm, ZnO NPs) for high-temperature applications. The approach consists of encapsulation of NPs into a nitrogen-doped carbon (NC) layer *in situ* grown from zeolitic imidazolate framework-8 on a Silicalite-1 support. The NC layer was established to control the size of ZnO NPs and to hinder their loss to a large extent at high temperatures. The designed catalysts exhibited high activity, selectivity, and on-stream stability in PDH. Propene selectivity of about 90% at 44.4% propane conversion was achieved at 600°C after nearly 6 h on stream.

INTRODUCTION

Propene is the second-largest building block of the chemical industry with a steadily increasing demand owing to its plentiful downstream applications. Stream cracking and fluid catalytic cracking (FCC) of various oil fractions are the most common methods for producing propene. These technologies have several drawbacks such as high-energy consumption and low selectivity to propene. In addition, metathesis of ethylene and 2-butenes (Mol and van Leeuwen, 2008) and non-oxidative propane dehydrogenation (PDH) (Caspary et al., 2008) have been developed for on-purpose propene production. The latter process is the most attractive technology because of the fast exploitation of shale gas providing an exciting opportunity for producing light olefins and aromatics (Wang and Li, 2017; Bruijnincx and Weckhuysen, 2013). For this reason, the PDH technology has attracted increasing attention of researchers from industry and academia around the world (Liu et al., 2016a, Sokolov et al., 2012; Kim et al., 2017; Hu et al., 2018; Zhu et al., 2017; Sattler et al., 2014a). From a fundamental viewpoint, PDH is also of great significance because it is a good model reaction for studying the fundamentals of the activation of C-H bond.

As PDH is a strongly endothermic reaction, it requires high temperatures (>500°C) to achieve industrially attractive degrees of propane conversion. Chromium-based (Mentasty et al., 1999; Weckhuysen and Schoonheydt, 1999) and platinum-based (Jiang et al., 2015; Shi et al., 2015; Li et al., 2017; Xiong et al., 2017) materials are the commercial catalysts used for this reaction, which have, however, shortcomings related to toxicity and high cost of the active components, respectively. To overcome them, a lot of efforts have been put into developing new kinds of alternative catalysts such as gallium-based (Kim et al., 2017; Choi et al., 2017; Sattler et al., 2014b), vanadium-based (Liu et al., 2016a, Hu et al., 2018; Sokolov et al., 2012), tin-based (Wang et al., 2016, 2017), and zirconium-based (Otroshchenko et al., 2015, Otroshchenko et al., 2016, Otroshchenko et al., 2017a, 2017b) materials. Owing to the recent developments in nanoscience and synthetic technologies, ZnO nanoparticles (ZnO NPs) or ZnO quantum dots as promising semiconductor materials were elaborately synthesized and are widely used in photocatalysis (Etacheri et al., 2012; He et al., 2014), photodetectors (Tang et al., 2018; Shao et al., 2013), degradation of organic pollutants (Akkari et al., 2017), and other low-temperature applications. ZnO-based materials are promising catalysts for PDH because of their costs, environment friendliness, and high efficiency to activate C-H bond (Sun et al., 2014; Schweitzer et al., 2014; Camacho-Bunquin et al., 2017; Liu et al., 2016b; Biscardi et al., 1998). However, ZnO is often unstable under reducing reaction conditions because of the formation

[1]State Key Laboratory of Heavy Oil Processing, China University of Petroleum, Beijing, Beijing 102249, P. R. China

[2]State Key Laboratory of Structural Chemistry, Fujian Institute of Research on the Structure of Matter, Chinese Academy of Sciences, Fuzhou, Fujian 350002, P. R. China

[3]Institutes of Physical Science and Information Technology, Anhui University, Hefei 230601, China

[4]Leibniz-Institut für Katalyse. V. an der Universität Rostock, Albert-Einstein-Strasse 29A, 18059 Rostock, Germany

[5]These authors contributed equally

[6]Lead Contact

*Correspondence: jianggy@cup.edu.cn (G.J.), bhge@ahu.edu.cn (B.G.), evgenii.kondratenko@catalysis.de (E.V.K.)

https://doi.org/10.1016/j.isci.2019.02.018

This is an open access article under the CC BY-NC-ND license (http://creativecommons.org/licenses/by-nc-nd/4.0/).

of metallic Zn, which melts at about 420°C. To improve the stability of ZnO at high temperatures, synthesis of composite oxides (Sun et al., 2014) and modification of ZnO with Pt (Liu et al., 2016b) have been proposed. To the best of our knowledge, ultrasmall ZnO NPs (<10 nm) have still not been studied in high-temperature (>420°C) reactions. The main reason is related to the difficulties in preparing catalysts possessing highly dispersed NPs with high stability against sintering and Zn/ZnO volatilization under reaction conditions (Anthrop and Searcy, 1964; Sirelkhatim et al., 2015).

Owing to their intriguing topologies and diverse functionalities, metal organic frameworks (MOFs) are widely used for gas separation (Hu et al., 2015; Cadiau et al., 2016; Rodenas et al., 2014), sensors (Campbell et al., 2015), and catalysis (Lee et al., 2009; Zhao et al., 2014; Zhao et al., 2016a, 2016b; Zhang et al., 2017). In the latter case, MOFs and metals@MOFs are applied in photocatalysis (Nasalevich et al., 2015), organic catalysis (Huang et al., 2017), and other reactions (Yang et al., 2016; Liu and Tang, 2013) as they possess highly dispersed metal sites. A recent attractive direction for MOF applications is their usage as precursors to generate highly dispersed metals or metal oxides@carbon materials (even single-site atoms@carbon material) (Chen et al., 2015, 2017; Yin et al., 2016). The formed carbon material or N-doped carbon material could isolate metal or metal oxide species, and M(metal)-N(N atom)-C(carbon material) bonds can be formed in some cases to prevent the catalytically active species from aggregation. In spite of this significant progress, reports on using non-metal heteroatoms in MOFs to synthesize stable metal and/or metal oxide-based catalysts at high temperatures are still rare. With this thought in mind, here we introduce a methodology for the preparation of composite catalysts with thermally stable ZnO NPs encapsulated into a nitrogen-doped carbon layer (NC layer) on the surface of Silicalite-1. The NC layer is formed through carbonizing zeolitic imidazolate framework-8 (ZIF-8, Zn(2-methylimidazole)$_2$) followed by leaching with nitric acid. Scanning transmission electron microscopy and H_2-temperature programmed reduction (H_2-TPR) revealed that the presence of N species in the NC layer is decisive for stabilizing the NPs at temperatures up to 700°C. The potential of the so-designed catalysts was validated for the PDH reaction at 600°C. Owing to the stabilizing effect of the NC layer on ZnO NPs, the catalysts showed high on-stream stability and activity.

RESULTS AND DISCUSSION

For the preparation of ZnO@NC and Silicalite-1 composite catalysts, Silicalite-1 was chosen as the support because it possesses high specific surface area and unique porosity (Figure S1), and it was synthesized according to the reference (Shen et al., 2013). Moreover, silica-based materials are typically used as supports for preparing selective PDH catalysts as they do not possess acidic sites, which are considered to negatively affect selectivity due to coke formation. To form a ZIF-8 layer on this support, $Zn(NO_3)_2 \cdot 6H_2O$ and 2-methylimidazole were added to a suspension of Silicalite-1 in methanol. After centrifuging and drying, the obtained solid material was carbonized at 700°C in N_2 atmosphere and denoted as ZnO@NC/S-1(0.0). The ZnO@NC/S-1(0.0) sample was further treated by nitric acid for partially dissolving ZnO species and thus generating more uniform ZnO NPs with smaller size. This material was abbreviated as ZnO@NC/S-1(x), where x stands for the concentration of the acid. Zn loading determined by inductively coupled plasma spectrum (ICP) in ZnO@NC/S-1(0.0) and ZnO@NC/S-1(1.0) was 2.8 wt % and 2.0 wt %, respectively. The X-ray diffraction patterns of as-synthesized ZIF-8 (Figure 1A) match well with the simulated pattern, confirming the formation of the ZIF-8 phase (Pan et al., 2011; Kuo et al., 2012). A reflex at 2θ of 7.3° characteristic for ZIF-8 is also presented in the diffractogram of Silicalite-1 coated with a ZIF-8 layer. The coated material maintained the typical MFI topological structure with good crystallinity after carbonizing the ZIF-8 layer followed by acid leaching process. No reflexes characteristic for bulk ZnO or NC material were observed. Thus the presence of large crystalline particles of ZnO and NC in the as-synthesized catalysts can be excluded. To derive an insight into the nature of carbon in the NC layer, we applied Raman spectroscopy. The obtained spectra of ZnO@NC/S-1(0.0) and ZnO@NC/S-1(1.0) are characterized by two evident bands at about 1,340 cm^{-1} and about 1,590 cm^{-1} (Figure 1B). These bands can be ascribed to the defective structure (D band) and graphitic carbon (G band), respectively (Lim et al., 2012; Zhang et al., 2014). The relatively low ratio of the D band intensity to that of the G band indicates the high degree of graphitization of the formed NC material. X-ray photoelectron spectroscopy (XPS) was applied to determine catalyst surface composition. All XPS signals were adjusted by the position of Si 1s with a binding energy of 103.3 eV. As seen in Figure 1C, two XPS signals at about 1,022 eV and about 1,045 eV are presented in the spectra of all catalysts and are characteristic for Zn $2p_{1/2}$ and Zn $2p_{3/2}$, respectively (Ma et al., 2011; Aksoy et al., 2012). However, in comparison with ZnO loaded on Silicalite-1 (ZnO/Silicalite-1, 1,022.2 eV), the Zn $2p_{1/2}$ binding energy for ZnO@NC/S-1(0.0) and ZnO@NC/S-1(1.0) is slightly shifted to lower values, i.e., 1,022.0 eV and 1,021.6 eV, accordingly. The energy shift may be caused by the electron donor property of the

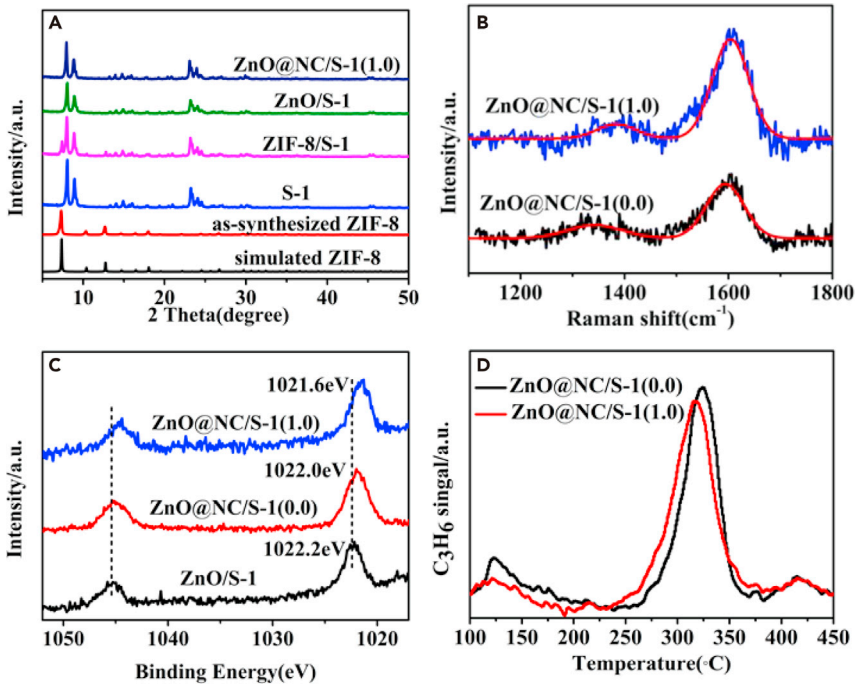

Figure 1. Physicochemical properties of as-synthesized catalysts

(A) X-ray diffraction patterns of as-synthesized catalysts.

(B) Raman spectra of ZnO@NC/S-1(x) samples.

(C) Zn 2p spectra of as-synthesized catalysts.

(D) Temperature-programmed desorption profiles of propene from ZnO@NC/S-1(x) samples.

See also Figures S2 and S3.

introduced NC layer. After HNO_3 leaching, the binding energy value is also shifted from 1,022.0 eV to 1,021.6 eV, which may be caused by decreasing ZnO content. Detailed N 1s spectra of ZnO@NC/S-1(0.0) and ZnO@NC/S-1(1.0) are presented in Figure S2. On their basis, three different kinds of N species were identified: pyridinic-N, pyrrolic-N, and graphitic-N. Their percentage distribution is given in Table 1. The profiles of temperature-programmed desorption of propene (C_3H_6-TPD) from these two samples are presented in Figures 1D and S3, and the temperature (T_{max}) of maximal desorption is given in Table 1. These data suggest that C_3H_6 adsorbs weaker on the ZnO@NC/S-1(1.0) sample than on the ZnO@NC/S-1(0.0) sample. Owing to electron-rich property of C_3H_6, it adsorbs more strongly on the ZnO@NC/S-1(0.0) sample with electron-deficient state (higher values of Zn binding energy) as confirmed by XPS results.

To determine the size of ZnO NPs, high-angle annular dark-field scanning transmission electron microscopy (STEM) and bright-field STEM were applied, and the corresponding representative images are shown in Figures 2A and 2B. It can be clearly seen that ZnO NPs are encapsulated into the NC layer. ZnO NPs in ZnO@NC/S-1(0.0) have a broad distribution with an average size of 4.0 nm. Treatment with 1 M HNO_3 results in a narrower distribution of ZnO NPs with an average size of 2.6 nm in ZnO@NC/S-1(1.0). This may be due to the partial dissolution of ZnO in HNO_3 as concluded from the ICP results shown in Table 1. To elucidate the factors determining the stability of ZnO NPs at high temperatures, the ZnO@NC/S-1(1.0) sample was treated in either a flow of pure N_2 (ZnO@NC/S-1(1.0)-N_2-700°C) or a mixture of 10 vol % H_2 in N_2 (ZnO@NC/S-1(1.0)-10 vol % H_2-700°C) at 700°C for 2 h. ZnO NPs are hardly visible (Figures 2A III, 2B III, and S4) in the sample treated in the H_2-containing mixture, and the ZnO loading is 0.4 wt %. The latter result suggests that most of ZnO was lost during 10 vol % H_2 treatment at 700°C. In contrast, ZnO NPs did not disappear after N_2 treatment (Figures 2A IV and 2B IV) as concluded from the fact that Zn loading decreased only slightly from 2.0 to 1.8 wt %. The size of Zn NPs also decreased from 2.6 to 2.0 nm. To derive an insight into the effect of H_2 treatment on the stability of ZnO NPs, H_2-TPR tests were additionally carried out using a fresh sample. When carefully analyzing the H_2-TPR results (Figure S5), no signal related to water could be identified, thus indicating that ZnO NPs could not be reduced upon

Samples	S_{BET} (m^2/g)	Zn Loading (wt %)[a]	r_{coke} ($g \cdot g^{-1}_{cat} \cdot h^{-1}$)[b]	T_{max} (°C)[c]	N Species[d]		
					Pyridinic N	Pyrrolic N	Graphitic N
ZnO/S-1	426	2.5	0.004	–	–	–	–
ZnO@NC/S-1(0.0)	351	2.8	0.10	324	32%	40%	28%
ZnO@NC/S-1(1.0)	370	2.0	0.01	316	48%	25%	27%

Table 1. Specific Surface Area (S_{BET}), Zn Loading, Rate of Coke Formation (r_{coke}), Temperature (T_{max}) of Maximal Propene Desorption, and Surface Distribution of Different N Species

See also Figures S1 and S9.

[a]Zn loading was determined by ICP.

[b]r_{coke} was calculated on the basis of thermogravimetric analysis (TGA) according to Equation 1. (See it in Supplemental Information)

[c]Determined from temperature-programmed profiles of propene desorption.

[d]Obtained through deconvolution of detailed N 1s peak in the XPS.

reductive catalyst treatment. As proven by *in situ* diffuse reflection infrared fourier transform spectrum (DRIFTs) analysis of the catalysts treated in different atmospheres and at different temperatures (Figure S6), no surface functional groups characteristic of aromatic C-N or C=N species could be identified after treatment at 700°C in H_2/N_2. Such species were, however, present after treatment in N_2. Thus we can conclude that N species could be removed in the form of NH_3 upon H_2 treatment at high temperatures (>650°C). Taking the above results into account, it can be confirmed that the N species can provide protective function for ZnO NPs to a large extent at high temperatures. Consequently, the aggregation and loss of ZnO could be prevented by carbon layer and N species, respectively. Such efficient preparation of ultrasmall ZnO NPs by encapsulating in NC material via post-treatment of MOFs thus presents a platform for maintaining potential stability in PDH at 600°C.

To check if and how the kind (ZnO@NC-based versus impregnated catalyst) of catalyst and the presence of N in NC layer affect catalytic performance in PDH, catalytic tests were performed at 600°C and atmospheric pressure. Propane conversion and propene selectivity as a function of time on stream are summarized in Figures 3 and S7. Poor catalytic performance of bare Silicalite-1 (S-1) as well as NC and S-1 (NC/S-1) composite material (Figure S7) indicates that the support and the NC material are inactive for PDH, whereas Zn-containing materials were active. Thus ZnO NPs should be the active species. However, catalytic activity depends on how this active component was introduced on the surface of Silicalite-1. For comparison, when a similar amount of ZnO (2.5 wt %) was introduced into Silicalite-1 by incipient wetness impregnation (ZnO/S-1), propane conversion was only 13.7% and the selectivity to propene was below 70% (Figure S7). When ZnO/S-1 was treated with 1 M HNO_3, the initial conversion of propane decreased from 13.7% to 6.9%, whereas the selectivity to propene slightly increased. The as-prepared ZnO@NC/S-1(x) composite catalysts performed significantly superior. This can be due to the presence of ultrasmall ZnO NPs. STEM analysis proved that the NPs were stable during the PDH. The size of ZnO NPs in spent ZnO@NC/S-1(1.0) did not change obviously (2.2 nm, Figures 2A V and 2B V). In addition, the conversion of propane and the selectivity to propene increased with an increase in the concentration of nitric acid used for catalyst leaching. Acidic treatment is also important for catalyst stability against deactivation. The higher the acid concentration, the higher the on-stream stability was (Figure S7). For example, the conversion of propane over ZnO@NC/S-1(0.0) dropped from 52.2% to 15.3% within 315 min on propane stream, whereas the corresponding values for ZnO@NC/S-1(1.0) were 56.4% and 44.4%. For the ZnO@NC/S-1(1.0) sample, the selectivity to propene maintained at about 90% during stability test. Other undesired gas-phase products were mainly methane, ethane, and ethene (Figure S8). The selectivity to propene over ZnO@NC/S-1(1.0) was also higher than that over ZnO@NC/S-1(0.0). Such phenomenon may be caused by a decrease in particle size of ZnO after acid catalyst treatment. According to previous studies on PDH reaction (Zhang et al., 2018; Zhu et al., 2015), undesired reactions are inhibited upon decreasing the size of catalytically active species. The amount of coke formed during the PDH reaction was quantitatively determined by thermogravimetric (TG) analysis (Figure S9) and used for calculating the average rate of coke deposition (Table 1). The lowest rate was obtained for ZnO/S-1 due to its very low PDH activity and consequently low concentration of propene responsible for coke formation. Importantly, the rate of coke deposition over ZnO@NC/S-1(1.0) is 10 times lower than that over the ZnO@NC/S-1(0.0) catalysts, although the samples operated with a similarly high initial activity. Taking into account the results of C_3H_6-TPD (Figure 1D) and TG tests, it can be concluded

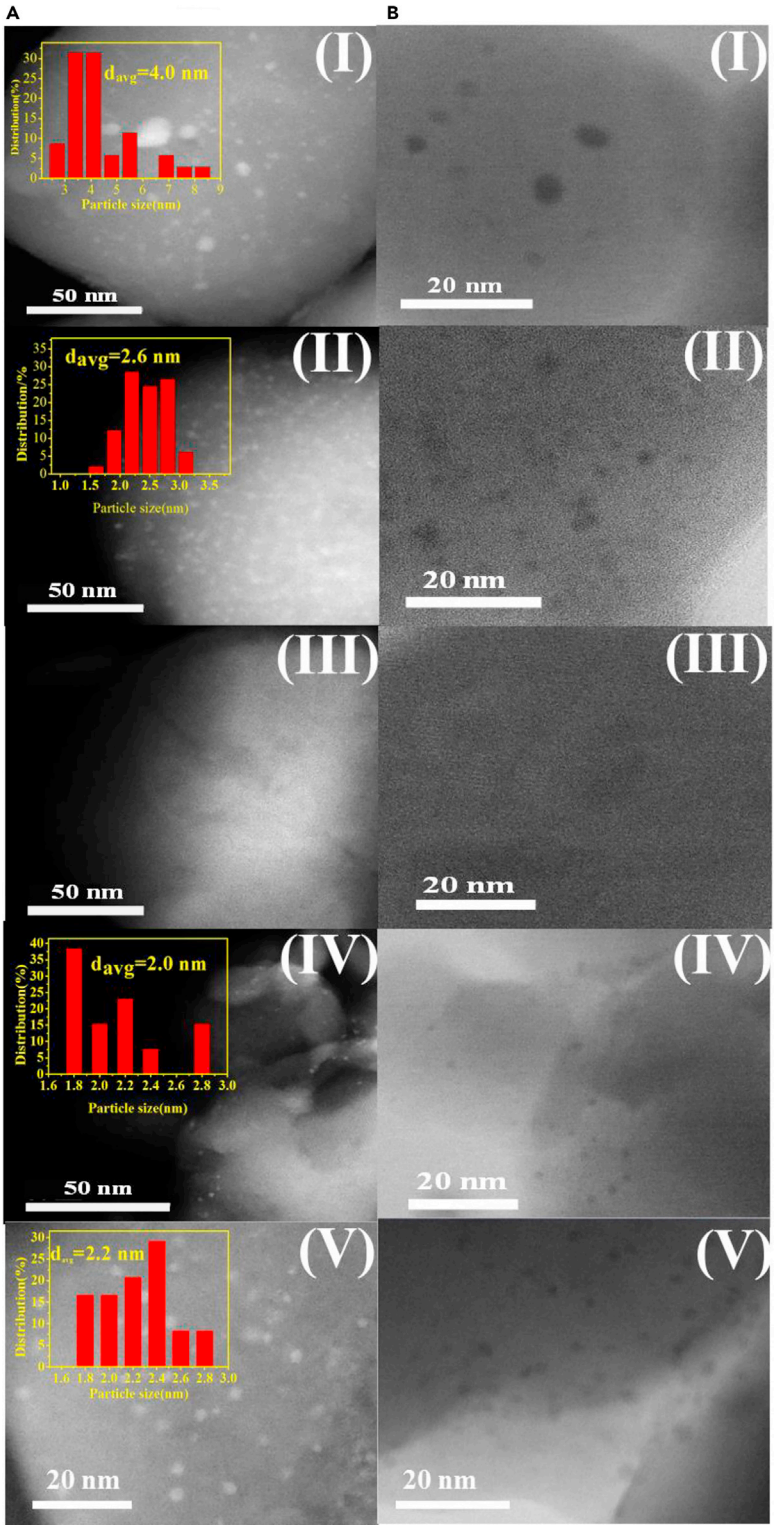

Figure 2. Electron microscopic characterization of as-prepared catalysts

(A) HAADF STEM images and (B) BF-STEM images of as-synthesized catalysts. (I) ZnO@NC/S-1(0.0), (II) ZnO@NC/S-1(1.0), (III) ZnO@NC/S-1(1.0)-10 vol % H_2-700°C, (IV) ZnO@NC/S-1(1.0)-N_2-700°C, (V) spent ZnO@NC/S-1(1.0) (Scale bars, 50 nm in A [I–IV] and 20 nm in A [V] and B [I–V[).

See also Figures S4–S6.

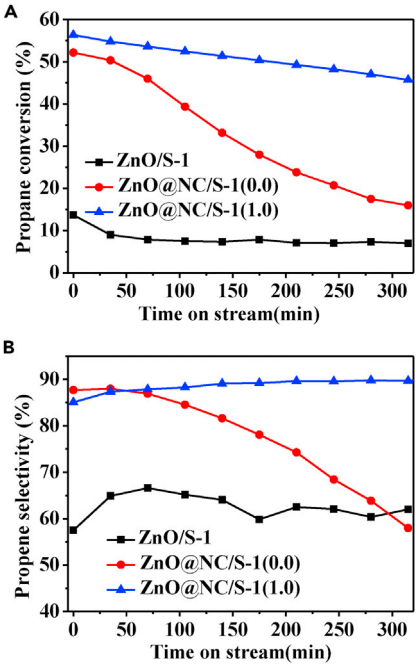

Figure 3. Catalytic performance of as-prepared catalysts

(A) Propane conversion and (B) propene selectivity. Reaction conditions: 0.2 g catalysts, 600°C, H_2: C_3H_8: N_2 = 1: 1: 5, N_2 flow rate was 7.5 mL/min.

See also Figures S7 and S8.

that C_3H_6 interacts weaker with ZnO@NC/S-1(1.0) than with ZnO@NC/S-1(0.0). As a consequence, appropriate adsorption/desorption properties of C_3H_6 species would effectively hinder their transformation into coke precursors (Jiang et al., 2015; Shi et al., 2015). On the basis of the results of carbon and ICP analysis of catalysts before and after reaction (Table 1 and Figure S9), reaction-induced carbon deposition should be the main reason for catalyst deactivation, which is slow over ZnO@NC/S-1(1.0). In addition, although the loss of ZnO has been hindered in the present case, it will also result in a drop in the activity to some extent. Unfortunately, when carrying out oxidative catalyst regeneration, not only carbon deposits but also NC layer will be oxidized, thus resulting in the loss of their protection function. The problem may be solved by selective coke removal by controlling combustion parameters. The related work is ongoing in our group.

In summary, a facile strategy was developed to prepare catalysts with ultrasmall ZnO NPs being stable up to 700°C. An NC layer *in situ* formed through carbonization of MOFs is used for encapsulation of such NPs and thus protects ZnO NPs from sintering and volatilization at high-temperature. The so-designed catalysts demonstrate high activity, selectivity, and on-stream stability in PDH. Such efficient utilization of MOFs via simple post-treatment for the construction of stable ZnO NPs may provide new insights into the design of highly effective metal oxide NPs and promote their catalytic applications.

Limitations of the Study

Additional characterization of the ZnO nanoparticles would be warranted, and regeneration of the catalyst would be also valuable.

METHODS

All methods can be found in the accompanying Transparent Methods supplemental file.

SUPPLEMENTAL INFORMATION

Supplemental Information can be found online at https://doi.org/10.1016/j.isci.2019.02.018.

ACKNOWLEDGMENTS

This work is supported by the National Natural Science Foundation of China (Grant Nos. 21878331, 91645108, 21802167, U1162117) and Science Foundation of China University of Petroleum, Beijing (Nos. C201604, 2462017YJRC002).

AUTHOR CONTRIBUTIONS

G.J., B.G., and E.V.K. designed and conceived this work; D.Z. and Y.L. contributed equally to this work and carried out the synthesis, characterization, and catalytic test. D.Z. wrote the manuscript, and Y.L., G.J., and E.V.K. revised the manuscript. S.H. and Y.Z. analyzed the catalytic results. R.L. and C.Y. performed the H_2-TPR measurements. B.G. carried out the STEM characterization. K.G. performed the *in situ* DRIFTs and part of ICP analysis. All the authors participated in the discussion of the results and the preparation of the paper.

DECLARATION OF INTERESTS

Y.L. has filed a patent application based on the work in this manuscript. All other authors declare no competing financial interests.

Received: August 6, 2018
Revised: November 15, 2018
Accepted: December 6, 2018
Published: March 29, 2019

REFERENCES

Akkari, M., Aranda, P., Mayoral, A., Garcia-Hernandez, M., Ben Haj Amara, A., and Ruiz-Hitzky, E. (2017). Sepiolite nanoplatform for the simultaneous assembly of magnetite and zinc oxide nanoparticles as photocatalyst for improving removal of organic pollutants. J. Hazard. Mater. *340*, 281–290.

Aksoy, S., Caglar, Y., Ilican, S., and Caglar, M. (2012). Sol-gel derived Li-Mg co-doped ZnO films: preparation and characterization via XRD, XPS, FESEM. J. Alloy. Compd. *512*, 171–178.

Anthrop, D.F., and Searcy, A.W. (1964). Sublimation and thermodynamic properties of zinc oxide. J. Phys. Chem. *68*, 2335–2342.

Biscardi, J.A., Meitzner, G.D., and Iglesia, E. (1998). Structure and density of active Zn species in Zn/H-ZSM5opane aromatization catalysts. J. Catal. *179*, 192–202.

Bruijnincx, P.C., and Weckhuysen, B.M. (2013). Shale gas revolution: an opportunity for the production of biobased chemicals? Angew. Chem. Int. Ed. *52*, 11980–11987.

Cadiau, A., Adil, K., Bhatt, P.M., Belmabkhout, Y., and Eddaoudi, M. (2016). A metal-organic framework-based splitter for separating propylene from propane. Science *353*, 137–140.

Camacho-Bunquin, J., Aich, P., Ferrandon, M., "Bean" Getsoian, A., Das, U., Dogan, F., Curtiss, L.A., Miller, J.T., Marshall, C.L., Hock, A.S., and Stair, P.C. (2017). Single-site zinc on silica catalysts for propylene hydrogenation and propane dehydrogenation: synthesis and reactivity evaluation using an integrated atomic layer deposition-catalysis instrument. J. Catal. *345*, 170–182.

Campbell, M.G., Sheberla, D., Liu, S.F., Swager, T.M., and Dinca, M. (2015). Cu_3(hexaiminotriphenylene)$_2$: an electrically conductive 2D metal-organic framework for chemiresistive sensing. Angew. Chem. Int. Ed. *54*, 4349–4352.

Caspary, K.J., Gehrke, H., Heinritz-Adrian, M., and Schwefer, M. (2008). Dehydrogenation of Alkanes. In Handbook of heterogeneous catalysis, *Vol. 7*, G. Ertl, H. Knözinger, F. Schüth, and J. Weitkamp, eds. (Wiley-VCH), p. 3206.

Chen, Y., Wang, C., Wu, Z., Xiong, Y., Xu, Q., Yu, S., and Jiang, H. (2015). From bimetallic metal-organic framework to porous carbon: high surface area and multicomponent active dopants for excellent electrocatalysis. Adv. Mater. *27*, 5010–5016.

Chen, Y., Ji, S., Wang, Y., Dong, J., Chen, W., Li, Z., Shen, R., Zheng, L., Zhuang, Z., Wang, D., and Li, Y. (2017). Isolated single iron atoms anchored on N-doped porous carbon as an efficient electrocatalyst for the oxygen reduction reaction. Angew. Chem. Int. Ed. *56*, 6937–6941.

Choi, S.W., Kim, W.G., So, J.S., Moore, J.S., Liu, Y., Dixit, R.S., Pendergast, J.G., Sievers, C., Sholl, D.S., Nair, S., and Jones, C.W. (2017). Propane dehydrogenation catalyzed by gallosilicate MFI zeolites with perturbed acidity. J. Catal. *345*, 113–123.

Etacheri, V., Roshan, R., and Kumar, V. (2012). Mg-doped ZnO nanoparticles for efficient sunlight-driven photocatalysis. ACS Appl. Mater. Interfaces *4*, 2717–2725.

He, W., Kim, H.K., Wamer, W.G., Melka, D., Callahan, J.H., and Yin, J. (2014). Photogenerated charge carriers and reactive oxygen species in ZnO/Au hybrid nanostructures with enhanced photocatalytic and antibacterial activity. J. Am. Chem. Soc. *136*, 750–757.

Hu, T., Wang, H., Li, B., Krishna, R., Wu, H., Zhou, W., Zhao, Y., Han, Y., Wang, X., Zhu, W., et al. (2015). Microporous metal-organic framework with dual functionalities for highly efficient removal of acetylene from ethylene/acetylene mixtures. Nat. Commun. *6*, 7328.

Hu, P., Lang, W., Yan, X., Chu, L., and Guo, Y. (2018). Influence of gelation and calcination temperature on the structure-performance of porous VO_X-SiO_2 solids in non-oxidative propane dehydrogenation. J. Catal. *358*, 108–117.

Huang, Y., Liang, J., Wang, X., and Cao, R. (2017). Multifunctional metal-organic framework catalysts: synergistic catalysis and tandem reactions. Chem. Soc. Rev. *46*, 126–157.

Jiang, F., Zeng, L., Li, S., Liu, G., Wang, S., and Gong, J. (2015). Propane dehydrogenation over Pt/TiO_2-Al_2O_3 catalysts. ACS Catal. *5*, 438–447.

Kim, W., So, J., Choi, S.W., Liu, Y., Dixit, R.S., Sievers, C., Sholl, D.S., Nair, S., and Jones, C.W. (2017). Hierarchical Ga-MFI catalysts for propane dehydrogenation. Chem. Mater. *29*, 7213–7222.

Kuo, C.H., Tang, Y., Chou, L.Y., Sneed, B.T., Brodsky, C.N., Zhao, Z., and Tsung, C.K. (2012). Yolk-shell nanocrystal@ZIF-8 nanostructures for gas-phase heterogeneous catalysis with selectivity control. J. Am. Chem. Soc. *134*, 14345–14348.

Lee, J., Farha, O.K., Roberts, J., Scheidt, K.A., Nguyen, S.T., and Hupp, J.T. (2009). Metal-organic framework materials as catalysts. Chem. Soc. Rev. *38*, 1450–1459.

Li, J., Li, J., Zhao, Z., Fan, X., Liu, J., Wei, Y., Duan, A., Xie, Z., and Liu, Q. (2017). Size effect of TS-1 supports on the catalytic performance of PtSn/TS-1 catalysts for propane dehydrogenation. J. Catal. *352*, 361–370.

Lim, S., Suh, K., Kim, Y., Yoon, M., Park, H., Dybtsev, D.N., and Kim, K. (2012). Porous carbon materials with a controllable surface area synthesized from metal-organic frameworks. Chem. Commun. *48*, 7447.

Liu, Y., and Tang, Z. (2013). Multifunctional nanoparticle@MOF core-shell nanostructures. Adv. Mater. *35*, 5819–5825.

Liu, G., Zhao, Z., Wu, T., Zeng, L., and Gong, J. (2016a). Nature of the active sites of VO_x/Al_2O_3 catalysts for propane dehydrogenation. ACS Catal. *6*, 5207–5214.

Liu, G., Zeng, L., Zhao, Z., Tian, H., Wu, T., and Gong, J. (2016b). Platinum-modified ZnO/Al_2O_3 for propane dehydrogenation: Minimized platinum usage and improved catalytic stability. ACS Catal. *6*, 2158–2162.

Ma, H., Han, J., Fu, Y., Song, Y., Yu, C., and Dong, X. (2011). Synthesis of visible light responsive ZnO-ZnS/C photocatalyst by simple carbothermal reduction. Appl. Catal. B Environ. *102*, 417–423.

Mentasty, L.R., Gorriz, O.F., and Cadus, L.E. (1999). Chromium oxide supported on different Al_2O_3 supports: catalytic propane dehydrogenation. Ind. Eng. Chem. Res. *39*, 396–404.

Mol, J.C., and van Leeuwen, P.W.N.M. (2008). Metathesis of Alkenes. In Handbook of heterogeneous catalysis, *Vol. 6*, G. Ertl, H. Knözinger, F. Schüth, and J. Weitkamp, eds. (Wiley-VCH), p. 3420.

Nasalevich, M.A., Becker, R., Ramos-Fernandez, E.V., Castellanos, S., Veber, S.L., Fedin, M.V., Kapteijn, F., Reek, J.N.H., Vlugt, J.I.v.d., and Gascon, J. (2015). Co@NH_2-MIL-125(Ti): cobaloxime-derived metal-organic framework-based composite for light-driven H_2 production. Energy Environ. Sci. *8*, 364–375.

Otroshchenko, T., Sokolov, S., Stoyanova, M., Kondratenko, V.A., Rodemerck, U., Linke, D., and Kondratenko, E.V. (2015). ZrO_2-based alternatives to conventional propane dehydrogenation catalysts: active sites, design, and performance. Angew. Chem. Int. Ed. *54*, 15880–15883.

Otroshchenko, T., Radnik, J., Schneider, M., Rodemerck, U., Linke, D., and Kondratenko, E.V. (2016). Bulk binary ZrO_2-based oxides as highly active alternative-type catalysts for non-oxidative isobutane dehydrogenation. Chem. Commun. *52*, 8164–8167.

Otroshchenko, T., Kondratenko, V.A., Rodemerck, U., Linke, D., and Kondratenko, E.V. (2017a). ZrO_2-based unconventional catalysts for non-oxidative propane dehydrogenation: factors determining catalytic activity. J. Catal. *348*, 282–290.

Otroshchenko, T., Kondratenko, V.A., Rodemerck, U., Linke, D., and Kondratenko, E.V. (2017b). Non-oxidative dehydrogenation of propane, n-butane, and isobutane over bulk ZrO_2-based catalysts: effect of dopant on the active site and pathways of product formation. Catal. Sci. Technol. *7*, 4499–4510.

Pan, Y., Liu, Y., Zeng, G., Zhao, L., and Lai, Z. (2011). Rapid synthesis of zeolitic imidazolate framework-8 (ZIF-8) nanocrystals in an aqueous system. Chem. Commun. *47*, 2071–2073.

Rodenas, T., Luz, I., Prieto, G., Seoane, B., Miro, H., Corma, A., Kapteijn, F., Xamena, F.X.L.i, and Gascon, J. (2014). Metal-organic framework nanosheets in polymer composite materials for gas separation. Nat. Mater. *14*, 48–55.

Sattler, J.J., Ruiz-Martinez, J., Santillan-Jimenez, E., and Weckhuysen, B.M. (2014a). Catalytic dehydrogenation of light alkanes on metals and metal oxides. Chem. Rev. *114*, 10613–10653.

Sattler, J.J., Gonzalez-Jimenez, I.D., Luo, L., Stears, B.A., Malek, A., Barton, D.G., Kilos, B.A., Kaminsky, M.P., Verhoeven, T.W., Koers, E.J., et al. (2014b). Platinum-promoted Ga/Al_2O_3 as highly active, selective, and stable catalyst for the dehydrogenation of propane. Angew. Chem. Int. Ed. *53*, 9251–9256.

Schweitzer, N.M., Hu, B., Das, U., Kim, H., Greeley, J., Curtiss, L.A., Stair, P.C., Miller, J.T., and Hock, A.S. (2014). Propylene hydrogenation and propane dehydrogenation by a single-site Zn^{2+} on silica catalyst. ACS Catal. *4*, 1091–1098.

Shao, D., Yu, M., Sun, H., Hu, T., Lian, J., and Sawyer, S. (2013). High responsivity, fast ultraviolet photodetector fabricated from ZnO nanoparticle-graphene core-shell structures. Nanoscale *5*, 3664–3667.

Shen, K., Qian, W., Wang, N., Su, C., and Wei, F. (2013). Fabrication of c-axis oriented ZSM-5 hollow fibers based on an in situ solid-solid transformation mechanism. J. Am. Chem. Soc. *41*, 15322–15325.

Shi, L., Deng, G., Li, W., Miao, S., Wang, Q., Zhang, W., and Lu, A. (2015). Al_2O_3 nanosheets rich in pentacoordinate Al^{3+} ions stabilize Pt-Sn clusters for propane dehydrogenation. Angew. Chem. Int. Ed. *54*, 13994–13998.

Sirelkhatim, A., Mahmud, S., Seeni, A., Kaus, N.H.M., Ann, L.C., Bakhori, S.K.M., Hasan, H., and Mohamad, D. (2015). Review on zinc oxide nanoparticles: antibacterial activity and toxicity mechanism. Nanomicro Lett. *7*, 219–242.

Sokolov, S., Stoyanova, M., Rodemerck, U., Linke, D., and Kondratenko, E.V. (2012). Comparative study of propane dehydrogenation over V-, Cr-, and Pt-based catalysts: time on-stream behavior and origins of deactivation. J. Catal. *293*, 67–75.

Sun, Y., Gao, C., Tao, L., Wang, G., Han, D., Li, C., and Shan, H. (2014). Zn-Nb-O catalysts for propylene production via catalytic dehydrogenation of propane. Catal. Commun. *50*, 73–77.

Tang, R., Han, S., Teng, F., Hu, K., Zhang, Z., Hu, M., and Fang, X. (2018). Size-controlled graphene nanodot arrays/ZnO hybrids for high-performance UV photodetectors. Adv. Sci. *5*, 1700334.

Wang, Q., and Li, R. (2017). Research status of shale gas: a review. Renew. Sustain Energy Rev. *74*, 715–720.

Wang, G., Zhang, H., Wang, H., Zhu, Q., Li, C., and Shan, H. (2016). The role of metallic Sn species in catalytic dehydrogenation of propane: active component rather than only promoter. J. Catal. *344*, 606–608.

Wang, G., Zhang, H., Zhu, Q., Zhu, X., Li, X., Wang, H., Li, C., and Shan, H. (2017). Sn-containing hexagonal mesoporous silica (HMS) for catalytic dehydrogenation of propane: an efficient strategy to enhance stability. J. Catal. *351*, 90–94.

Weckhuysen, B.M., and Schoonheydt, R.A. (1999). Alkane dehydrogenation over supported chromium oxide catalysts. Catal. Today *51*, 223–232.

Xiong, H., Lin, S., Goetze, J., Pletcher, P., Guo, H., Kovarik, L., Artyushkova, K., Weckhuysen, B.M., and Datye, A.K. (2017). Thermally stable and regenerable platinum-tin clusters for propane dehydrogenation prepared by atom trapping on ceria. Angew. Chem. Int. Ed. *56*, 8986–8991.

Yang, Q., Xu, Q., Yu, S., and Jiang, H. (2016). Pd nanocubes@ZIF-8: Intergration of plasmon-driven photothermal conversion with a metal-organic framework for efficient and selective catalysis. Angew. Chem. Int. Ed. *55*, 3685–3689.

Yin, P., Yao, T., Wu, Y., Zheng, L., Lin, Y., Liu, W., Ju, H., Zhu, J., Hong, X., Deng, Z., et al. (2016). Single cobalt atoms with precise N-coordination as superior oxygen reduction reaction catalysts. Angew. Chem. Int. Ed. *55*, 10800–10805.

Zhang, L., Su, Z., Jiang, F., Yang, L., Qian, J., Zhou, Y., Li, W., and Hong, M. (2014). Highly graphitized nitrogen-doped porous carbon nanopolyhedra derived from ZIF-8 nanocrystals as efficient electrocatalysts for oxygen reduction reactions. Nanoscale *6*, 6590–6602.

Zhang, Y., Guo, J., Shi, L., Zhu, Y., Hou, K., Zheng, Y., and Tang, Z. (2017). Tunable chiral metal organic frameworks toward visible light-driven asymmetric catalysis. Sci. Adv. *3*, e1701162.

Zhang, Y., Zhao, Y., Otroshchenko, T., Lund, H., Pohl, M., Rodemerck, U., Linke, D., Jiao, H., Jiang, G., and Kondratenko, E.V. (2018). Control of coordinatively unsaturated Zr sites in ZrO_2 for efficient C-H bond activation. Nat. Commun. *9*, 3794.

Zhao, M., Deng, K., He, L., Liu, Y., Zhao, H., and Tang, Z. (2014). Core-shell palladium nanoparticle@metal-organic frameworks as multifunctional catalysts for cascade reactions. J. Am. Chem. Soc. *136*, 1738–1741.

Zhao, M., Yuan, K., Wang, J., Li, G., Guo, J., Gu, L., Hu, W., Zhao, H., and Tang, Z. (2016a). Metal-organic frameworks as selectivity regulators for hydrogenation reactions. Nature *539*, 76–80.

Zhao, S., Wang, Y., Dong, J., He, C., Yin, H., An, P., Zhao, K., Zhang, X., Gao, C., Zhang, L., et al. (2016b). Ultrathin metal-organic framework nanosheets for electrocatalytic oxygen evolution. Nat. Energy *1*, 16184.

Zhu, J., Yang, M., Yu, Y., Zhu, Y., Sui, Z., Zhou, X., Holmen, A., and Chen, D. (2015). Size-dependent reaction mechanism and kinetics for propane dehydrogenation over Pt catalysts. ACS Catal. *5*, 6310–6319.

Zhu, Y., An, Z., Song, H., Xiang, X., Yan, W., and He, J. (2017). Lattice-confined Sn (IV/II) stabilizing raft-like Pt clusters: high selectivity and durability in propane dehydrogenation. ACS Catal. *7*, 6973–6978.

ISCI, Volume *13*

Supplemental Information

ZnO Nanoparticles Encapsulated in Nitrogen-Doped Carbon Material and Silicalite-1 Composites for Efficient Propane Dehydrogenation

Dan Zhao, Yuming Li, Shanlei Han, Yaoyuan Zhang, Guiyuan Jiang, Yajun Wang, Ke Guo, Zhen Zhao, Chunming Xu, Ranjia Li, Changchun Yu, Jian Zhang, Binghui Ge, and Evgenii V. Kondratenko

Supporting Information

1 Transparent Methods

1.1 Experimental

1.1.1 Chemicals

Tetraethyl orthosilicate (Sinopharm Chemical Reagent Co., Ltd), $Zn(NO_3)_2 \cdot 6H_2O$ (Sinopharm Chemical Reagent Co., Ltd), 2-Methylimidazole (Energy Chemical), tetrapropylammonium hydroxide (Shanghai Cairui Chemical Engineering Technology Co., Ltd) and nitric acid (Beijing Chemical Industry Group Co. Ltd) were used as received without any further purification.

1.1.2 Synthesis of Silicalite-1 zeolite

Silicalite-1 was synthesized according to the reference (Shen et al. 2013) but with some modifications. In a typical process, measured amount of tetrapropylammonium hydroxide (25wt%, 48.8 g) was blended in deionized water (25.92 g), after 10 minutes agitating, 50 g of tetraethyl orthosilicate was added to the above mixture with continuous stirring and the solution was aged for additional 6 h. The solution was then placed in 200 mL Teflon stainless-steel autoclaves under static conditions at 100^{o}C for 2 days. The solid product was obtained by centrifugation, washed several times with deionized water, dried overnight at 110^{o}C, and calcined in air at 550^{o}C for 6 h to remove structure-directing agent, and the as-prepared Silicalite-1 was abbreviated as S-1.

1.1.3 Synthesis of Silicalite-1 with ZIF-8

1 g of Silicalite-1 was dispersed in 25 ml methanol with agitating and ultrasound condition to form a milk white suspension. Then 0.3 g of $Zn(NO_3)_2 \cdot 6H_2O$ was added into the slurry under agitating condition for 1 h, and 1.75 g of 2-methylimidazole was added into the mixture, after that, the mixture was stirred at room temperature for 6 h. The Silicalite-1 with ZIF-8 coating catalyst was obtained by centrifugation and dried overnight at 60^{o}C. Single ZIF-8 sample was synthesized as similar as above processes without Silicalite-1.

1.1.4 Carbonization of Silicalite-1 with ZIF-8

Carbonization process of Silicalite-1 with ZIF-8 layer was carried out in N_2 atmosphere at 700^{o}C for 2 h with a heating rate of 5^{o}C/min, and the sample were denoted as ZnO@NC/S-1(0.0). For ZnO@NC/S-1(0.0) sample, the amount of Zn is 2.8 wt % which was measured by ICP-OES (Inductively Coupled Plasm-Optical Emission Spectrum).

1.1.5 Leaching process

1 g of ZnO@NC/S-1(0.0) sample was dispersed in HNO_3 solution with different concentrations (0.3 M/0.5 M/1 M) under agitating condition at room temperature for 30 min. Then the products were collected by filtration, and washed with copious amount of water until the pH value was ~7. And then dried at 100^{o}C overnight, and the samples were denoted as ZnO@NC/S-1(x), where x means the concentration of HNO_3. For ZnO@NC/S-1(1.0) sample, the content of Zn is 2.0 wt% measured by ICP-OES. All the samples were pressed and sieved to particles in the range of 40-60 mesh.

1.1.6 Synthesis of ZnO/Silicalite-1

The ZnO/Silicalite-1 sample with desirable Zn content was synthesized by incipient wetness impregnation, and the as-synthesized catalyst was dried at 100°C for overnight, then it was calcinated at 700°C for 2 h, and the obtained sample was denoted as ZnO/S-1. The amount of Zn is 2.5 wt % which was measured by ICP-OES. The obtained ZnO/S-1 sample was leached by 1M HNO_3 at room temperature for 30 min, denoted as ZnO/S-1(1.0).

1.1.7 Preparation of NC/S-1 sample

The NC/S-1 sample was synthesized by calcinating the ZnO@NC/S-1(0.0) sample at 900°C for 2 h in N_2 flow with a heating rate of 5°C/min.

1.1.8 Treatment of ZnO@NC/S-1(1.0) sample under different gas flow

The 40-60 mesh of ZnO@NC/S-1(1.0) sample was treated under 10 vol%H_2-N_2 and N_2 in a 6 mm quartz tube, then the process lasted for 2 h at 700°C with a heating rate of 5°C/min and cooled down to room temperature, and the sample was denoted as ZnO@NC/S-1(1.0)-gas flow-temperature. The ZnO loadings are determined by ICP, which are 1.8 wt% and 0.4 wt% after N_2 and 10 vol%H_2-N_2 treatment, respectively.

1.2 Characterization

The catalysts were characterized by various techniques. X-ray diffraction (XRD) patterns were obtained from an X-ray diffractometer (Bruker, D8 Advance) with Cu Kα radiation at a voltage of 40 kV, a current of 40 mA and the 2θ was at the range of 5-90°.

Textual properties of catalysts were measured by N_2 adsorption at 77 K on an automatic adsorption instrument (Micromeritics Instrument, Tristar II 3020). The samples were outgassed at 350°C for 4 h before measurement.

Temperature programmed desorption of propene (C_3H_6-TPD) was carried out on Xianquan TP-5076 equipment with TCD detector. Typically, 100 mg catalyst was pre-treated on N_2 flow (20 ml/min) at 600°C for 1h. Subsequently, the catalyst was cooled down to room temperature (about 30°C) to adsorb propene for 30 min. Then, the C_3H_6-TPD profile was obtained at a heating rate of 10°/min from 100°C to 450°C.

H_2-temperature programmed reduction was carried out in an in-house developed setup (equipped mass spectrum detector). 0.3 g of samples was pretreated under Ar flow (40 ml/min) at 420°C or 620°C. After cooling down to room temperature, the profile was obtained when the Ar flow was switched to 10%H_2-Ar (20 ml/mim) with a heating rate of 15°C/min to 750°C and stayed 30 min.

X-ray photoelectron spectroscopy was carried out on Thermo Fisher K-Alpha. And all the peaks were adjusted by the position of Si 1s with a binding energy of 103.3 eV.

The HAADF-STEM and BF-STEM images were obtained by 200KeV JEOL ARM 200.

TG analysis was carried out on Mettler-Toledo TGA/DSC-1. The profile was obtained at O_2 flow with a heating rate of 10°C/min. And the coke deposition rate was calculated by below equation:

$$\text{Coke deposition rate} = [m_{(\text{after reaction})} - m_{(\text{before reaction})}]/[m_{(\text{catalyst})} * \text{reaction time}] \quad \text{eq1}$$

Here, $m_{(\text{after reaction})}$ and $m_{(\text{before reaction})}$ is the mass of coke and carbon material, respectively, $m_{(\text{catalyst})}$ is the mass of catalyst, time is the reaction time。

1.3 Catalytic test

The catalytic performances of as-synthesized catalysts for propane dehydrogenation were carried out in quartz tube with fixed bed. Before evaluation, the catalysts were pretreated on N_2 flow at reaction temperature 600ºC for 30 min. Then switched the C_3H_8, H_2 and N_2 with ratio of 1:1:5, and N_2 flow rate is 7.5 ml/min. A gas chromatograph equipped aluminum capillary column and flame ionization detector (FID) was employed to analyze all products. Propane conversion, propene selectivity and yield were calculated according to the following equations:

$$X_{(C_3H_8)} = \frac{m_{(C_3H_8,\,inlet)} - m_{(C_3H_8,\,outlet)}}{m_{(C_3H_8,\,inlet)}} \times 100\%$$

$$S_{(C_3H_6)} = \frac{m_{(C_3H_6,\,outlet)}}{\sum m_{(C_iH_j)\,products}} \times 100\%$$

$$Y_{(C_3H_6)} = S_{(C_3H_6)} \times X_{(C_3H_8)}$$

$m(C_3H_{8,inlet})$ and $m(C_3H_{8,outlet})$ stand for the mass fraction of the C_3H_8 before and after reaction.

$m(C_iH_j)$ means the mass fraction of products.

2 Additional characterization of the catalysts

2.1 BET

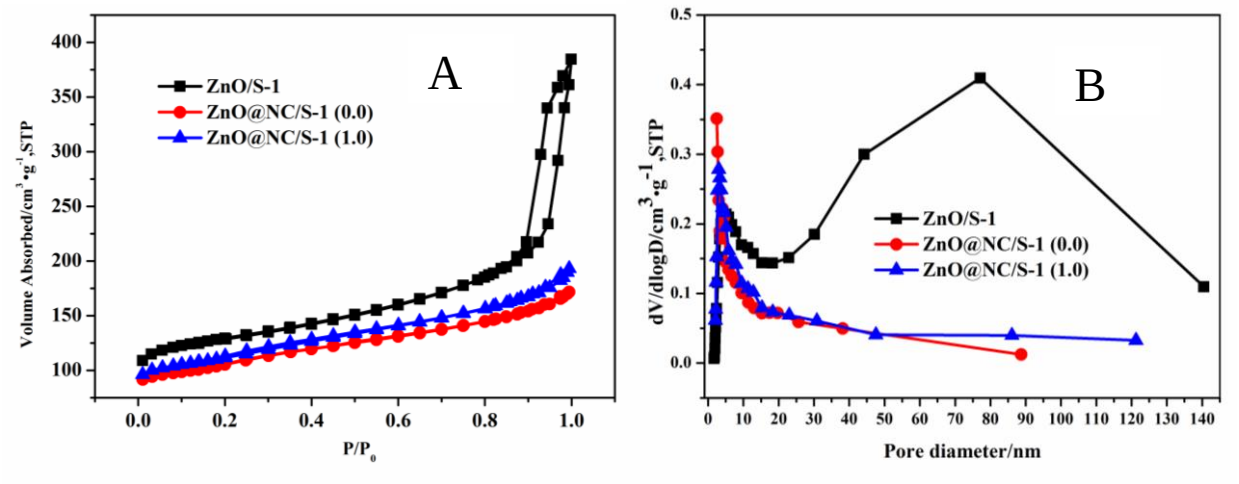

Figure S1 (A) N_2 adsorption-desorption isotherms, (B) pore size distribution (BJH adsorbed branch). Related to Table 1

2.2 XPS

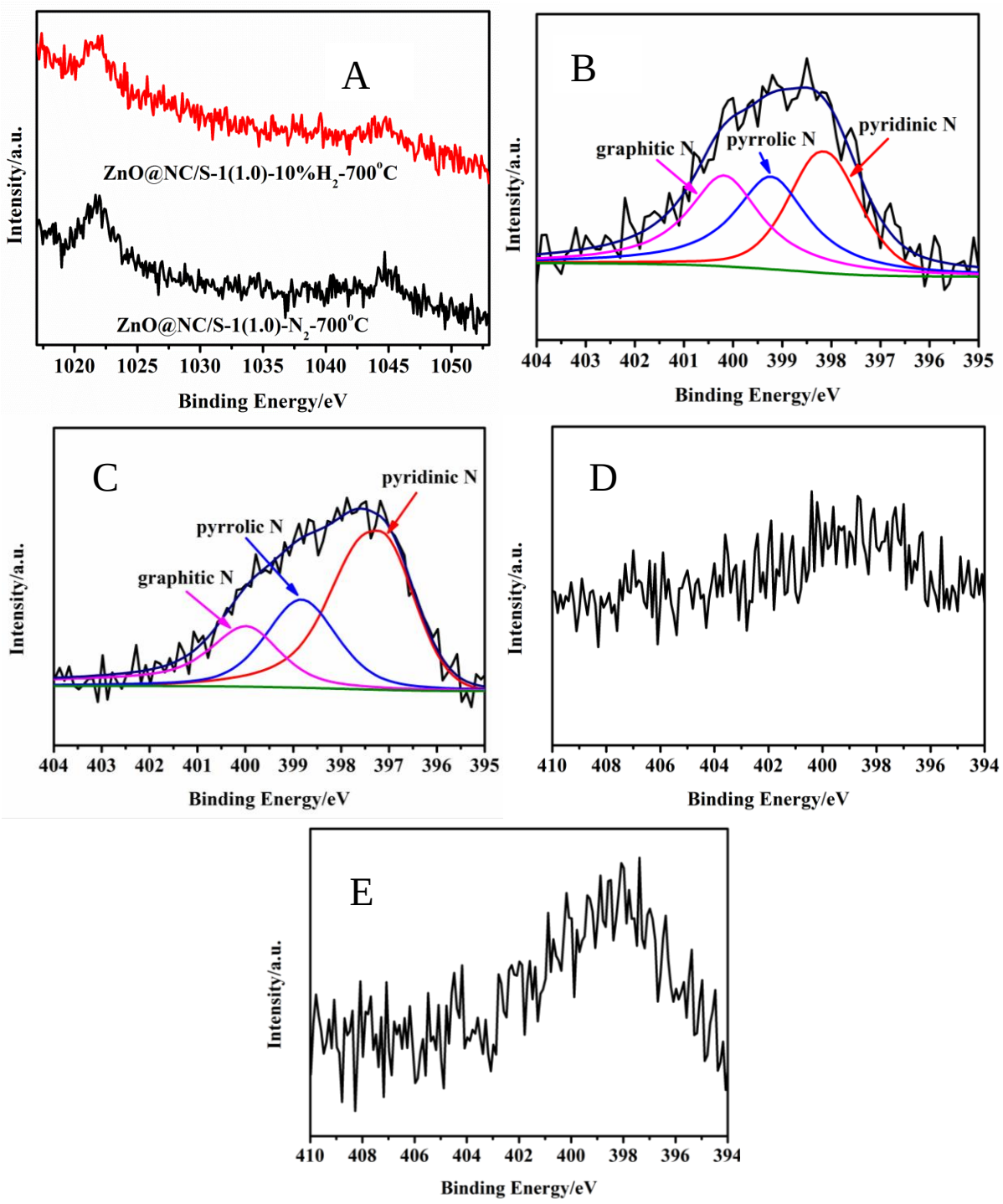

Figure S2. (A) Zn 2p core level spectra of post-treated sample over ZnO@NC/S-1(1.0); (B), (C), (D) and (E) N 1s core level spectra of ZnO@NC/S-1(0.0), ZnO@NC/S-1(1.0), ZnO@NC/S-1(1.0)-N_2-700ºC and ZnO@NC/S-1(1.0)-10 vol%H_2-700ºC, respectively. For ZnO@NC/S-1(1.0)-10 vol%H_2-700ºC sample (Figure S2A), the peaks of Zn $2p_{1/2}$ and Zn $2p_{3/2}$ are contributed to ZnO, and the peaks are ambiguous, speculating that the content of ZnO is very low on the catalyst surface after 10% H_2 treatment at 700ºC(0.4 wt% of ZnO loading). Related to Figure 1

2.3 C_3H_6-TPD

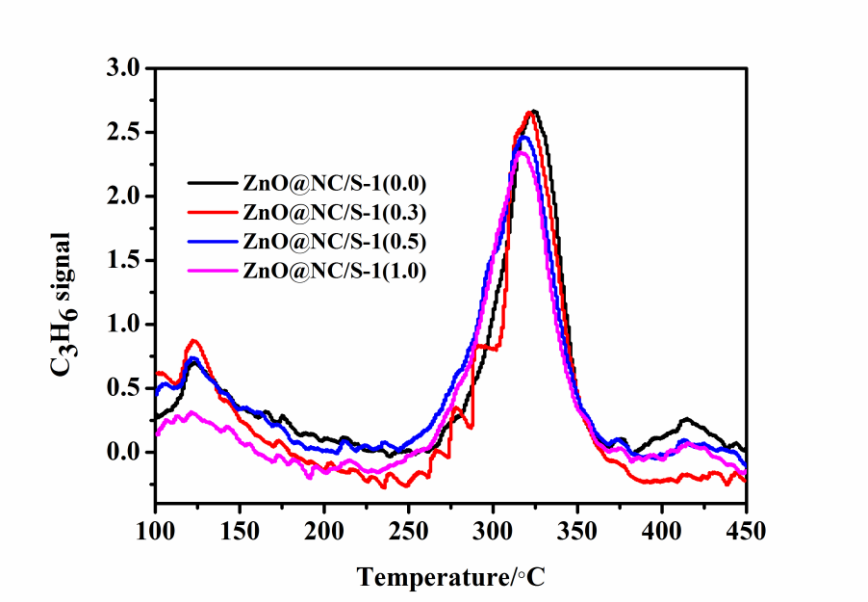

Figure S3 The C_3H_6-TPD profiles of ZnO@NC/S-1(x) samples. For ZnO@NC/S-1(x), the peak position was shifted to a lower temperature after acid leaching with increasing concentration of nitric acid, indicating that the interaction between the C_3H_6 and catalysts was weakened. Related to Figure 1

2.4 STEM

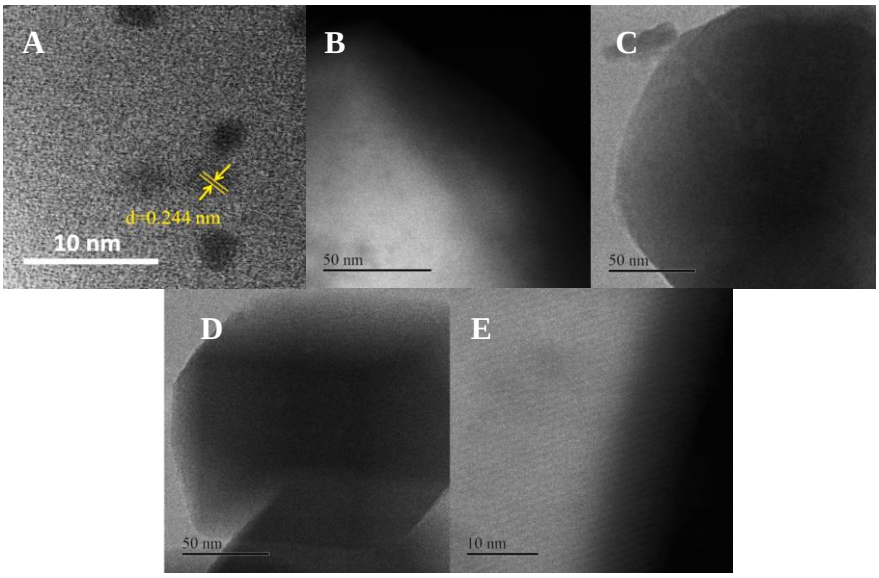

Figure S4 STEM images of (A) ZnO@NC/S-1(1.0) with lattice fringe of ZnO NPs and (B~E) ZnO@NC/S-1(1.0)-10%H_2-700°C sample. Related to Figure 2

2.5 H_2-TPR

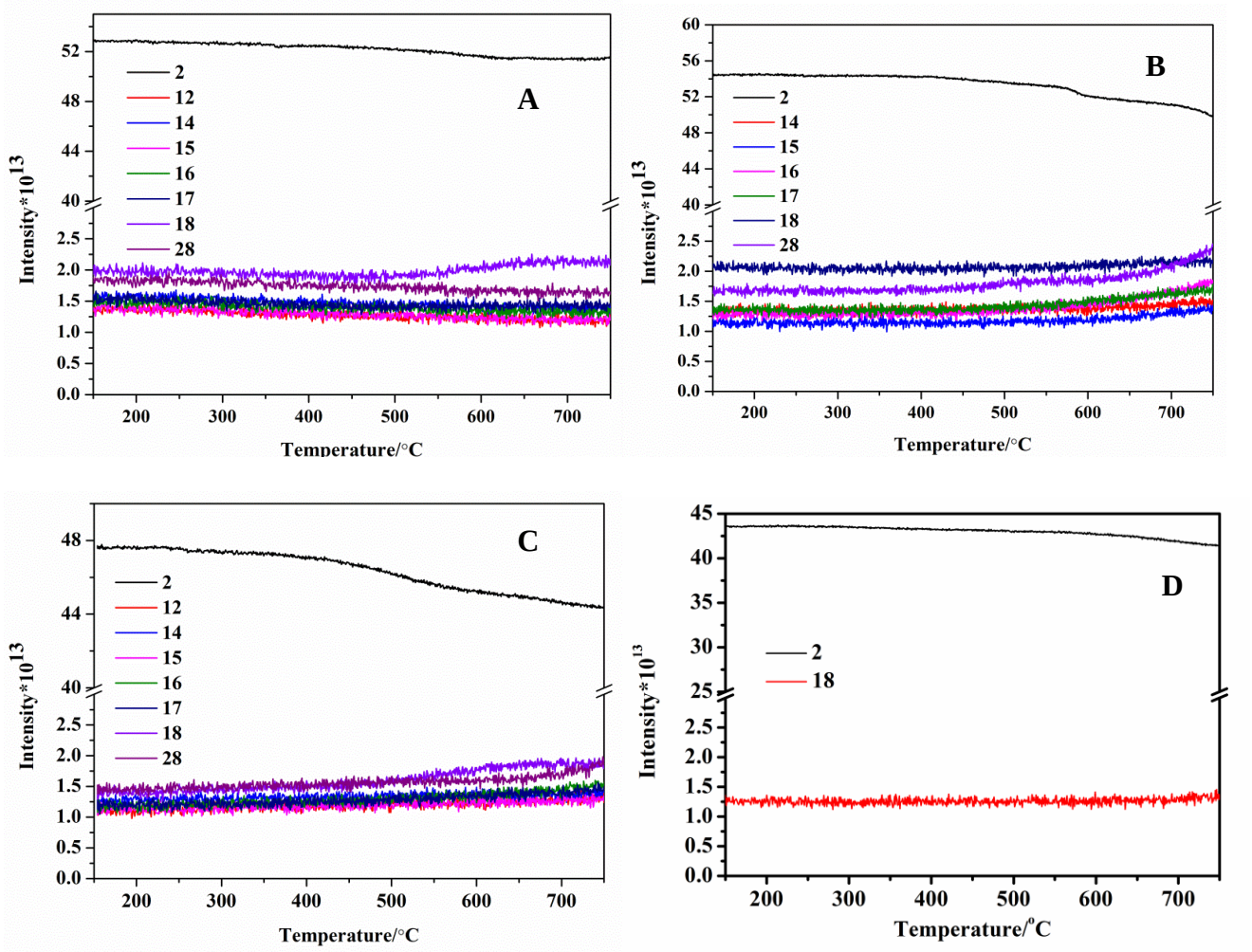

Figure S5 H_2-TPR profiles of as-synthesized catalysts. (A) ZnO/S-1 (B) ZnO@NC/S-1(0.0), (C) ZnO@NC/S-1(1.0), (A), (B) and (C) samples were pretreated at 420°C. (D) ZnO@NC/S-1(1.0) sample was pretreated at 620°C. For ZnO/S-1 and ZnO@NC/S-1(1.0) sample, a slight amount of H_2O was detected by mass spectrum detector (MS). In order to identify the source of H_2O during the reducing reaction, the ZnO@NC/S-1(1.0) sample was pretreated at 620°C (Figure S5D), and it was found that no water was detected by MS, indicating that the water was produced by dehydration of Si-OH on the Silicalite-1. For the ZnO@NC/S-1(0.0) and ZnO@NC/S-1(1.0) samples (Figure S5B and C), NH_3 could be formed during the H_2 reducing process at high temperature (>650°C). Related to Figure 2

2.6 *In-situ* DRIFTS

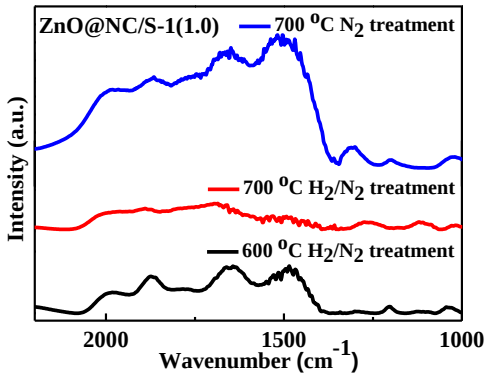

Figure S6 *In-situ* DRIFTs spectra of ZnO@NC/S-1(1.0) under different treatment conditions. Related to Figure 2

2.7 Catalytic performances

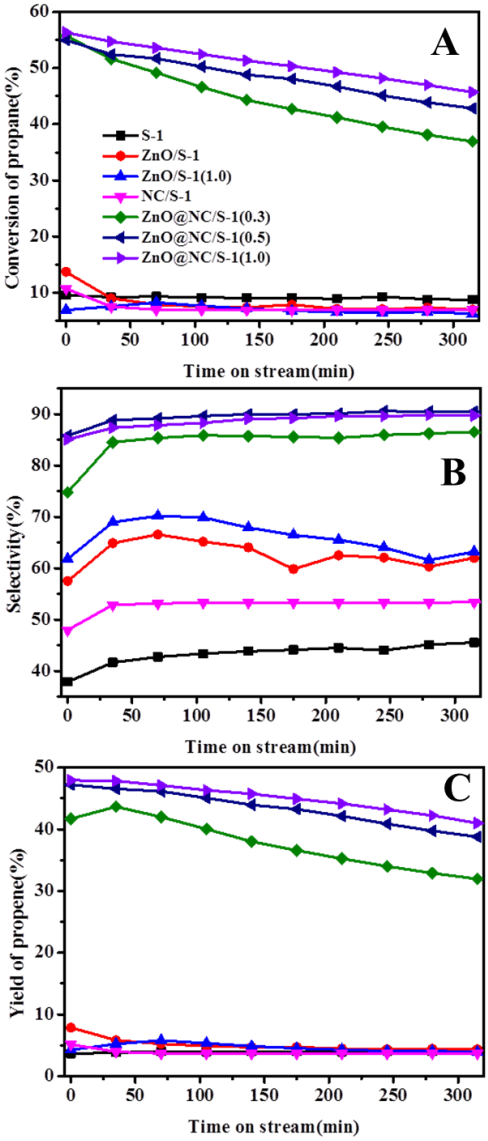

Figure S7 (A) propane conversion, (B) propene selectivity, (C) propene yield. Reaction conditions: 0.2 g of catalyst, 600°C, $V(H_2):V(C_3H_8):V(N_2)=1:1:5$, N_2 flow rate: 7.5 ml/min. Related to Figure 3

2.8 The original gas chromatogram

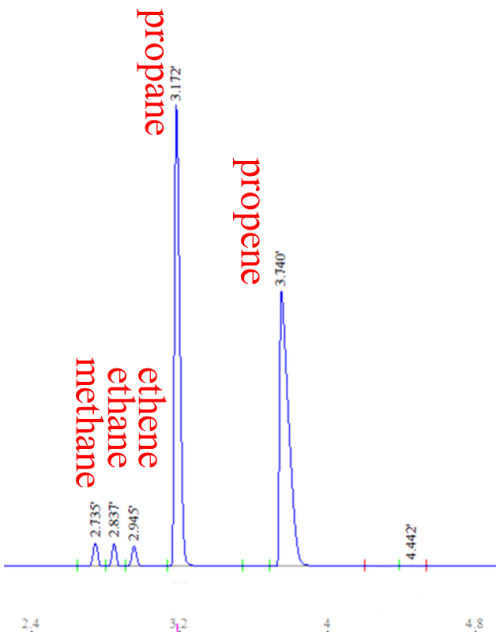

Figure S8 The original gas chromatogram. Related to Figure 3

2.9 TG

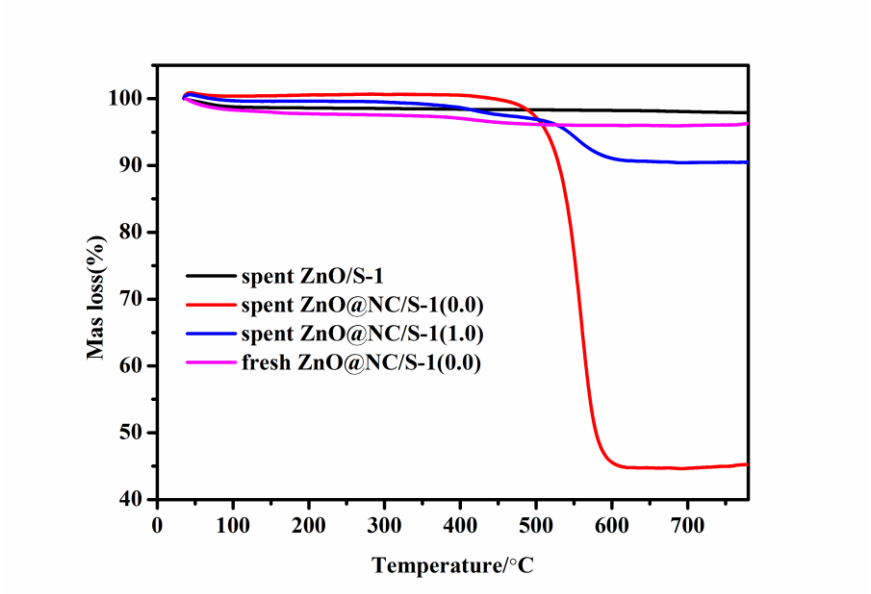

Figure S9 The TG profiles of fresh catalyst and spent catalyst. Related to Table 1